RSC Advances

PAPER

View Article Online
View Journal | View Issue

Cite this: *RSC Adv.*, 2021, **11**, 2701

Photocatalytic degradation of organic pollutants through conjugated poly(azomethine) networks based on terthiophene–naphthalimide assemblies†

Matías J. Alonso-Navarro, [ab] Jesús Barrio, [cd] Sergio Royuela, [ab] Neeta Karjule, [c] M. Mar Ramos, [b] José Ignacio Martínez, *[e] Menny Shalom *[c] and José L. Segura *[a]

Received 9th December 2020
Accepted 30th December 2020

DOI: 10.1039/d0ra10379a

rsc.li/rsc-advances

A conjugated poly(azomethine) network based on ambipolar terthiophene–naphthalimide assemblies has been synthesized and its electrochemical and UV-vis absorption properties have been investigated. The network has been found to be a promising candidate for the photocatalytic degradation of organic pollutants in aqueous media.

Due to the rapid growth of urbanization and intensive industrialization, pollution has evolved into a serious concern that produces a great negative impact on human health and the environment.[1,2] Therefore, many efforts are currently devoted to addressing environmental remediation through the degradation and removal of hazardous contaminants.[3–5] In this regard, photocatalysis has been identified as a suitable approach for environmental remediation given that it is an energy efficient technique that does not require chemical input and does not produce sludge residue.[6] In recent years, organic semiconducting polymers have evolved into a new type of metal-free and heterogeneous photocatalyst suitable for solar-energy utilization.[7] The modularity of organic polymers allows the efficient tunning of their electronic and optical properties by bottom-up organic synthesis through the choice of suitable monomeric building blocks.[8–10] Within this context, there is a growing demand for new organic polymeric semiconductors carefully designed to have suitable energy levels of the frontier orbitals, an appropriate bandgap and good intrinsic charge mobility.[11]

For the design of suitable polymeric semiconductors for photocatalysis, it is not only important that the photocatalysts absorb light in the visible light range but also an efficient dissociation of the photogenerated charge carriers is required. The combination of electron-poor acceptor (A) and electron-rich donor (D) moieties in the polymer structure may prevent a fast recombination process following photoexcitation.[12] In addition, it has been found that polymers networks bearing conjugated moieties may exhibit π-stacked columns that can facilitate charge transport.[13]

In this respect, molecular and polymeric materials based on the combination of oligothiophene[14,15] and naphthalimide moieties[16,17] connected through conjugated linkers have shown to be very effective in order to efficiently tune their frontier orbital levels and produce tunable organic semiconductors with good charge transport properties.[18–24] As an example, in Fig. 1 is depicted the structure of **NIP-3T**, an ambipolar organic semiconductor, for which the one-electron HOMO–LUMO excitation consists of the displacement of the electron density from the HOMO, primarily localized on the oligothiophene fragment, to the LUMO, localized on the naphthalimide unit.[25]

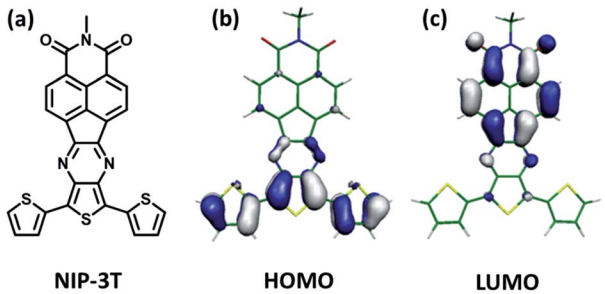

Fig. 1 (a) Monomer containing an electron donor terthiophene system directly conjugated with an electron acceptor naphthalimide moiety through a conjugated pyrazine linker (**NIP-3T**). (b) HOMO and (c) LUMO computed orbital topologies for **NIP-3T**.[25]

[a]*Department of Organic Chemistry, Complutense University of Madrid, Faculty of Chemistry, Madrid 28040, Spain. E-mail: segura@ucm.es*

[b]*Chemical and Environmental Technology Department, Univ. Rey Juan Carlos, Móstoles, 28933, Spain*

[c]*Department of Chemistry, Ilse Katz Institute for Nanoscale Science and Technology, Ben-Gurion University of the Negev, Beer-Sheva 8410501, Israel. E-mail: mennysh@bgu.ac.il*

[d]*Department of Materials, Imperial College London, Royal School of Mines, London SW72AZ, England*

[e]*Department of Nanostructures and Low-Dimensional Materials, Institute of Materials Science of Madrid (ICMM-CSIC), 28049 Madrid, Spain*

† Electronic supplementary information (ESI) available. See DOI: 10.1039/d0ra10379a

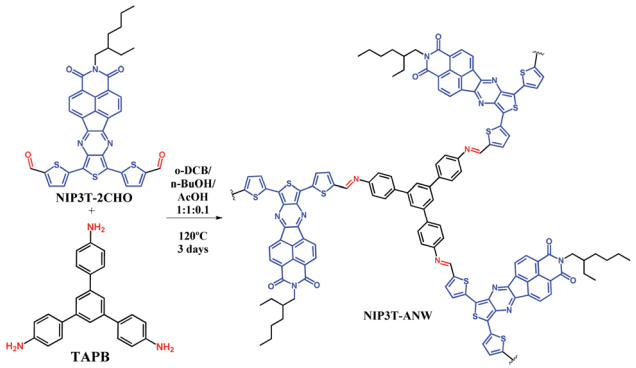

Scheme 1 Schematic representation of the synthesis of **NIP3T-ANW**.

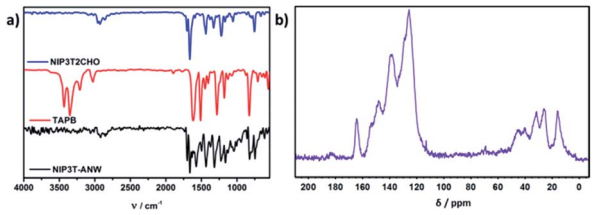

Fig. 2 (a) IR spectra of **NIP3T2CHO** (blue), **TAPB** (red) and **NIP3T-ANW** (black). (b) Solid-state ^{13}C CP-MAS NMR spectrum of **NIP3T-ANW**.

Among conjugated polymers, poly(azomethine)s have found application as organic semiconductors in heterogeneous photocatalysis because of their π-conjugated system and suitable band levels matching the redox window of water.[26] The incorporation of D–A monomeric assemblies into poly(azomethine) networks represents an efficient strategy to obtain ambipolar polymeric networks with tunable frontier orbital levels for photocatalytic applications. Thus, in this communication we report the synthesis of a novel donor–acceptor poly(azomethine) network (**NIP3T-ANW**, Scheme 1) based on **NIP-3T** monomers. The potential of this system as photodegrading agent for the elimination of contaminant organic dyes in aqueous media is also explored.

The synthesis of the macromolecular poly(azomethine) network **NIP3T-ANW** is acomplished through Schiff-base reactions between trigonal monomers endowed with amine functionalities (**TAPB**,[27] Scheme 1) and linear naphthalimide–thiophene-based monomers endowed with complementary aldehyde functional groups (**NIP3T2CHO**,[24] Scheme 1). Typically, both monomers were dissolved in an *o*-dichlorobenzene/*n*-butanol/acetic acid (1 : 1 : 0.1) mixture, which was then heated at 120 °C under solvothermal reaction conditions for 72 h. A black solid was obtained which was insoluble in common solvents such as water, acetone, THF, toluene or chlorinated solvents like dichloromethane or chloroform. The obtained solid was washed several times with THF to remove the starting materials and low-molecular weight by-products. After drying under vacuum, a black solid was obtained. The yield, as determined by weight, was 98%.

To investigate the chemical nature of the material, as well as to determine the conversion of the functional groups after the reaction, we have employed attenuated total reflectance Fourier transform infrared (ATR-FTIR) spectroscopy (Fig. 2). The bands arising from the NH_2 stretching (3000–3400 cm^{-1}) and NH_2 deformation (1650 cm^{-1}) vibrations of the primary amine group of **TAPB** and the signals from the aldehyde groups of **NIP3T2CHO** around 2870 (C–H stretching) and 1663 cm^{-1} (C=O stretching) are virtually absent in the **NIP3T-ANW** spectrum. In addition, a prominent new band is found at 1573 cm^{-1}, which can be assigned to the C=N stretching vibration of the imine linkages within the newly formed poly(azomethine) network.[28–30]

Solid-state ^{13}C cross-polarization magic angle spinning NMR (^{13}C CP-MAS NMR) spectrum (Fig. 2) reveals the characteristic imide signals of the 1,8-naphthalimide moiety at 164.4 ppm, as well as the signal corresponding to the imine carbon at 154 ppm and a signal at 148 ppm which can be assigned to the aromatic carbon neighbouring the nitrogen of the C=N group. The absence of the sp^2 carbons from the **NIP3T2CHO** [24] aldehyde functionalities above 180 ppm satisfactorily confirms the condensation between the aldehyde and the amine derivatives.

Due to the rigidity and geometry of the building blocks, the imine linkers could be ideally generated in such a way that result in a canonical layered hexagonal structure[31] as predicted by theoretical calculations (Fig. S1 and S2†). However, in the actual framework, X-ray diffraction (XRD) measurements indicate that the material is mainly amorphous with only some ordered regions, as indicated by the good agreement between the weak and broad diffraction peaks observed at 2θ values larger than 3 and those predicted by calculations for the ideal canonical layered hexagonal structure (Fig. S3†). In this regard, **NIP3T-ANW** was submitted to an exfoliation process following a previously described protocol[32] for the exfoliation of two-dimensional polymers (see ESI† for details). The exfoliated material was analysed by dynamic light scattering (DLS) showing a monomodal size distribution of *ca.* 400 nm (Fig. S4†) and transmission electron microscopy (TEM) reveals a sheet-like structural aspect (Fig. S5†).

Thermogravimetric analysis of the poly(azomethine) network **NIP3T-ANW** shows that the degradation starts at around 450 °C and only 40% weight loss is observed at 700 °C (Fig. S6†). This thermal stability is significantly higher than that observed for **NIP3T** (Fig. 1), the analogous molecular system based on terthiophene connected with naphthalimide through pyrazine for which the degradation starts at 200 °C (Fig. S6†).[22,25]

In photocatalysis mediated by semiconductors, electron–hole pairs (excitons) are generated after light absorption and afterwards dissociate into free charge carriers that can be utilized for redox reactions[33,34] such as CO_2 fixation,[35] water splitting[36] or organic mineralization.[37] Some of the crucial factors that make the photocatalytic process favourable are the levels of conduction and valence as well as the width of the band gap.[38–40] Thus, in order to characterize these parameters, the electrochemical and optical properties of **NIP3T-ANW** have been analysed.

The electrochemical properties of **NIP3T** and **NIP3T-ANW** were studied by cyclic voltammetry (Fig. 3). Both materials show ambipolar redox behaviour in which the reversible reduction processes are characteristic of the naphthalimide unit, while the oxidation processes can be ascribed to the conjugated oligothiophene moiety.[19–22,24] For **NIP3T-ANW**, the first reversible reduction wave (−1.29 V) is shifted to less negative values in comparison with **NIP-3T** (−1.41 V). On the other hand, the first oxidation half wave potential for **NIP3T** is observed at +0.41 V and for **NIP3T-ANW** at +0.44 V. These shifts agree with the electron acceptor ability of the imine linker.

The absorption spectrum of **NIP3T-ANW** as determined by UV-vis diffuse reflectance spectroscopy (UV-vis DRS, Fig. 3) shows a strong absorption in all the UV-vis range, extending even to the near infrared. This broad absorption is red-shifted in comparison with the one observed for **NIP3T** (Fig. 3), which reflects the formation of the new polymer network with an extended conjugation through the alpha positions of the terthiophenes.

Using the corresponding cut-off wavelengths, the optical band gaps E_g found for **NIP3T** and **NIP3T-ANW** are 1.59 and 1.42 eV respectively. This optical result suggests that the incorporation of the **NIP3T** core into an extended conjugated system efficiently harvests photons from the visible range, even extending into the near IR region.

To shed some light into the degree of crystallinity of the synthesized **NIP3T-ANW** network, we have carried out a battery of density functional theory (DFT)-based calculations with the QUANTUM ESPRESSO plane-wave DFT simulation code[41] (see details in ESI†). We have considered periodic boundary conditions to obtain a fully-relaxed ground-state crystal structure. Optimization of the cell-shape and size, simultaneously to the relaxation of the structure, reveals a hexagonal 2D lattice with an optimized parameter of 48.46 Å. Different interlayer stacking fashions have been tested, with only one yielding a good agreement with the experimental diffractogram from 2θ values >3°. The most favourable stacking predicted by theory consists in an intermediate configuration between the perfectly eclipsed and staggered configurations, with an interlayer distance of 3.42 Å, and permits an adequate accommodation of the layers profiting adjacent pores. Details on the structure can be found in the ESI.†

Additionally, we have computed the electronic band diagram of the obtained crystal structure along the high-symmetry k-path Γ → K → M → Γ, revealing a wide-gap (1.91 eV) semiconducting character, with rather dispersive valence and conduction bands, mainly resembling the molecular HOMO and LUMO of the molecular building blocks (see Fig. S7†). Besides, computed time-dependent DFT (TDDFT) UV-vis spectrum manifests an excellent agreement with the experimental UV-vis spectra (Fig. S8†). A broad and pronounced peak-feature is obtained between 600 and 800 nm, centred at around 720 nm (1.7 eV), which agrees with the optical gap of 1.6 eV found for **NIP3T** from Fig. 3a. This feature corresponds to electronic transitions between the valence and conduction bands, with an energy difference of around 0.2 eV between the optical and the electronic gap, which indicates that charge relaxation in excited states is not much significative. The good agreement between theoretical predictions on the canonically periodic computed system and the experimental evidences seems to justify the presence of some high-crystallinity regions from the synthesis.

The band gap of a semiconductor material and the reduction and oxidation potentials are key parameters which determine its light-harvesting properties and types of reaction that can be conducted and therefore the overall photo-catalytic activity. A shift in the adsorption edge of a semiconductor towards longer wavelengths implies a narrower band gap and the efficient harvesting of a wider photons range.[42] **NIP3T-ANW** seems to be an appealing material to be utilized as photocatalyst given (i) the optimal light harvesting properties as shown by the optical characterization, (ii) the efficient generation of electron–hole pairs owing to the insertion of terthiophene moieties, and (iii) the right energy band positions for the material.[7] We therefore evaluated the photocatalytic activity of **NIP3T-ANW** under white light for the degradation of a model organic pollutant (Rhodamine B dye, **RhB**) in aqueous solution.[43] In the absence of catalyst, **RhB** remains stable in solution under illumination (Fig. 4a and S9†). However, in presence of **NIP3T-ANW** nearly 90% of **RhB** in an aqueous solution is degraded after 120 min, showing the enhanced catalytic activity of the material (Fig. 4a and S10†). Furthermore, a good stability is shown upon 4 straight catalytic cycles (Fig. 4b, S11 and S12†). In contrast, in the presence of the **NIP3T** moiety, only a 55% degradation of **RhB** is observed in the same timeframe (Fig. 4a and S11†).

In the photocatalytic degradation of organic pollutants, they are typically broken down through the attack of superoxide and hydroxyl species, formed when atmospheric oxygen reacts with photogenerated electrons or when water or OH ions are oxidized by holes, respectively.[44] Additionally, electron–hole pairs (or excitons) can directly reduce or oxidize organic

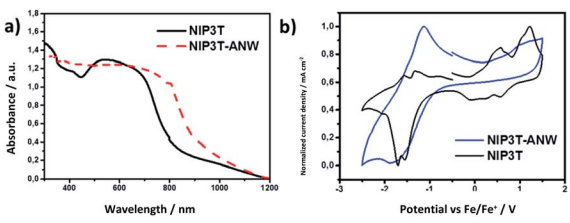

Fig. 3 (a) The UV-vis DRS spectra of NIP3T and NIP3T-ANW. (b) Cyclic voltammetry of the NIP3T monomer and the corresponding polymer.

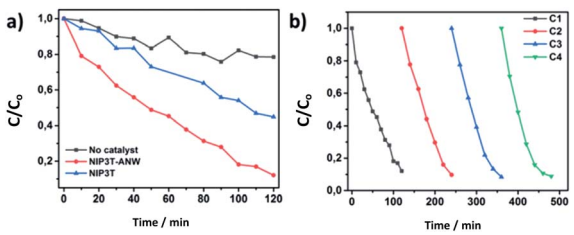

Fig. 4 RhB degradation curves. (a) Comparison between the degradation effect of NIP3T, NIP3T-ANW and without catalyst. (b) NIP3T-ANW stability after four recycling cycles.

pollutants in aqueous environments. Consequently, the evaluation of the photodegradation mechanism of organic pollutants, despite challenging, can provide meaningful insights about the nature of a semiconductor photocatalyst.[45] With the aim of evaluating the photodegradation mechanism we performed the measurements in the presence of different scavengers, namely an aqueous solution of $AgNO_3$ (100 mg L^{-1}), which captures photogenerated electrons, or triethanolamine (TEOA), which traps photogenerated holes (Fig. S13†).[46,47] In the presence of Ag^+ we could observe that the photocatalytic efficiency is enhanced, while the addition of TEOA quenched the performance, therefore suggesting that holes are the active specie in the photodegradation mechanism (Fig. S14†).

In summary, we have presented an approach towards the incorporation of D–A π-conjugated monomeric assemblies into poly(azomethine) networks to yield a purely organic semiconductor for the photocatalytic degradation of organic pollutants in aqueous media. The poly(azomethine) network benefits from a straightforward poly(condensation) approach which favourably competes with the elaborate high-temperature protocols applied for the preparation of inorganic materials. This work enriches the family of donor–acceptor organic semiconductor networks and, given its modular nature, paves the way for the development of a promising family of materials for photocatalytic applications.

Conflicts of interest

There are no conflicts to declare.

Acknowledgements

This work was financially supported by MINECO (MAT2016-77608-C3-2-P), MICINN (PID2019-106268GB-C33) and the UCM (INV.GR.00.1819.10759). MJAN gratefully acknowledges Universidad Rey Juan Carlos for a predoctoral contract. JIM acknowledges financial support by MINECO (MAT2017-85089-C2–1-R), Comunidad de Madrid *via* Programa de Investigación Tecnologías 2018 (No. FOTOART-CM S2018/NMT-4367), and the Innovation Program under grant 881603 (GrapheneCore3-graphene-based disruptive technologies). MS acknowledges the Minerva Center No. 117873 for funding.

Notes and references

1 R. P. Schwarzenbach, B. I. Escher, K. Fenner, T. B. Hofstetter, C. A. Johnson, U. von Gunten and B. Wehrli, *Science*, 2006, **313**, 1072–1077.
2 C. G. Daughton and T. A. Ternes, *Environ. Health Perspect.*, 1999, **107**, 907–938.
3 F. Chen, W. An, L. Liu, Y. Liang and W. Cui, *Appl. Catal., B*, 2017, **217**, 65–80.
4 W. Deng, H. Zhao, F. Pan, X. Feng, B. Jung, A. Abdel-Wahab, B. Batchelor and Y. Li, *Environ. Sci. Technol.*, 2017, **51**, 13372–13379.
5 P. Li, B. Zhun, X. Wang, P. Liao, G. Wang, L. Wang, Y. Guo and W. Zhang, *Environ. Sci. Technol.*, 2017, **51**, 14368–14378.
6 V. Vimonses, B. Jin, C. W. K. Chow and C. Saint, *Water Res.*, 2010, **44**, 5385–5397.
7 G. Zhang, Z.-A. Lan and X. Wang, *Angew. Chem., Int. Ed.*, 2016, **55**, 15712–15727.
8 L. Wang, Y. Wan, Y. Ding, S. Wu, Y. Zhang, X. Zhang, G. Zhang, Y. Xiong, X. Wu, J. Yang and H. Xu, *Adv. Mater.*, 2017, **29**, 1702428.
9 Z.-A. Lan, Y. Fang, Y. Zhang and X. Wang, *Angew. Chem., Int. Ed.*, 2018, **57**, 470–474.
10 R. S. Sprick, B. Bonillo, R. Clowes, P. Guiglion, N. J. Brownbill, B. J. Slater, F. Blanc, M. A. Zwijnenburg, D. J. Adams and A. I. Cooper, *Angew. Chem., Int. Ed.*, 2016, **55**, 1792–1796.
11 S. Xu, H. Sun, M. Addicoat, B. P. Biswal, F. He, S. Park, S. Paasch, T. Zhang, W. Sheng, E. Brunner, Y. Hou, M. Richter and X. Feng, *Adv. Mater.*, 2021, **33**, 2006274.
12 X. Fan, L. Zhang, R. Cheng, M. Wang, M. Li, Y. Zhou and J. Shi, *ACS Catal.*, 2015, **5**, 5008–5015.
13 E. Jin, Z. Lan, Q. Jiang, K. Geng, G. Li, X. Wang and D. Jiang, *Chem*, 2019, **5**, 1632–1647.
14 L. Zhang, N. S. Colella, B. P. Cherniawski, S. C. B. Mannsfeld and A. L. Briseno, *ACS Appl. Mater. Interfaces*, 2014, **6**, 5327–5343.
15 A. Mishra, C.-Q. Ma and P. Bäuerle, *Chem. Rev.*, 2009, **109**, 1141–1276.
16 A. Nowak-Król, K. Shoyama, M. Stolte and F. Würthner, *Chem. Commun.*, 2018, **54**, 13763–13772.
17 S. Kumar, J. Shukla, Y. Kumar and P. Mukhopadhyay, *Org. Chem. Front.*, 2018, **5**, 2254–2276.
18 J. L. Segura, H. Herrera and P. Bäuerle, *J. Mater. Chem.*, 2012, **22**, 8717–8733.
19 R. P. Ortiz, H. Herrera, R. Blanco, H. Huang, A. Facchetti, T. J. Marks, Y. Zheng and J. L. Segura, *J. Am. Chem. Soc.*, 2010, **132**, 8440–8452.
20 A. Riaño Carnerero, G. López Espejo, M. J. Mancheño Real, B. Eckstein, R. C. González-Cano, F. S. Melkonyan, A. Facchetti, T. J. Marks, J. Casado, J. T. López Navarrete, J. L. Segura and R. Ponce Ortiz, *J. Mater. Chem. C*, 2017, **5**, 9439–9450.
21 A. de la Peña, I. Arrechea-Marcos, M. J. Mancheño, M. C. Ruiz Delgado, J. T. López Navarrete, J. L. Segura and R. Ponce Ortiz, *Chem.–Eur. J.*, 2016, **22**, 13643–13652.
22 I. Arrechea-Marcos, P. de Echegaray, M. J. Mancheño, M. C. Ruiz Delgado, M. M. Ramos, J. A. Quintana, J. M. Villalvilla, M. A. Díaz-García, J. T. López Navarrete, R. Ponce Ortiz and J. L. Segura, *Phys. Chem. Chem. Phys.*, 2017, **19**, 6206–6215.
23 T. F. Otero, J. Arias-Pardilla, H. Herrera, J. L. Segura and C. Seoane, *Phys. Chem. Chem. Phys.*, 2011, **13**, 16513–16515.
24 M. J. Alonso-Navarro, A. Harbuzaru, P. de Echegaray, I. Arrechea-Marcos, A. Harillo-Baños, A. de la Peña, M. M. Ramos, J. T. López Navarrete, M. Campoy-Quiles, R. Ponce Ortiz and J. L. Segura, *J. Mater. Chem. C*, 2020, **8**, 15277–15289.
25 R. Ponce Ortiz, H. Herrera, M. J. Mancheño, C. Seoane, J. L. Segura, P. Mayorga Burrezo, J. Casado, J. T. López

Navarrete, A. Facchetti and T. J. Marks, *Chem.–Eur. J.*, 2013, **19**, 12458–12467.
26 M. G. Schwab, M. Hamburger, X. Feng, J. Shu, H. W. Spiess, X. Wang, M. Antonietti and K. Müllen, *Chem. Commun.*, 2010, **46**, 8932–8934.
27 A. de la Peña Ruigómez, D. Rodríguez-San-Miguel, K. C. Stylianou, M. Cavallini, D. Gentili, F. Liscio, S. Milita, O. M. Roscioni, M. L. Ruiz-González, C. Carbonell, D. Maspoch, R. Mas-Ballesté, J. L. Segura and F. Zamora, *Chem.–Eur. J.*, 2015, **21**, 10666–10670.
28 D. Sek, A. Iwan, B. Jarzabek, B. Kaczmarczyk, J. Kasperczyk, Z. Mazurak, M. Domanski, K. Karon and M. Lapkowski, *Macromolecules*, 2008, **41**, 6653–6663.
29 H. Niu, Y. Huang, X. Bai, X. Li and G. Zhang, *Mater. Chem. Phys.*, 2004, **86**, 33–37.
30 G.-S. Liou, H.-Y. Lin, Y.-L. Hsieh and Y.-L. Yang, *J. Polym. Sci., Part A: Polym. Chem.*, 2007, **45**, 4921–4932.
31 J. L. Segura, M. J. Mancheno and F. Zamora, *Chem. Soc. Rev.*, 2016, **45**, 5635–5671.
32 P. García-Arroyo, M. P. Arrieta, D. Garcia-Garcia, R. Cuervo-Rodríguez, V. Fombuena, M. J. Mancheño and J. L. Segura, *Polymer*, 2020, **196**, 122466.
33 F. Opoku, K. K. Govender, C. G. C. E. van Sittert and P. P. Govender, *Adv. Sustainable Syst.*, 2017, **1**, 1700006.
34 X. Chen, S. Shen, L. Guo and S. S. Mao, *Chem. Rev.*, 2010, **110**, 6503–6570.
35 K. Xu, Y. Dai, B. Ye and H. Wang, *Dalton Trans.*, 2017, **46**, 10780–10785.
36 T. Sick, A. G. Hufnagel, J. Kampmann, I. Kondofersky, M. Calik, J. M. Rotter, A. Evans, M. Döblinger, S. Herbert, K. Peters, D. Böhm, P. Knochel, D. D. Medina, D. Fattakhova-Rohlfing and T. Bein, *J. Am. Chem. Soc.*, 2018, **140**, 2085–2092.
37 H. Ma, M. Wei, F. Jin, T. Chen and Y. Ma, *J. Phys. Chem. C*, 2019, **123**, 24626–24633.
38 K. Li, L. Wang, Z. Chen, X. Yang, Y.-X. Yu, W.-D. Zhang, Y. Wang, Y. Shi, K. P. Loh and Q.-H. Xu, *Adv. Funct. Mater.*, 2020, **30**, 2005106.
39 W.-J. Ong, L.-L. Tan, Y. H. Ng, S.-T. Yong and S.-P. Chai, *Chem. Rev.*, 2016, **116**, 7159–7329.
40 J. Fu, J. Yu, C. Jiang and B. Cheng, *Adv. Energy Mater.*, 2018, **8**, 1701503.
41 P. Giannozzi, S. Baroni, N. Bonini, M. Calandra, R. Car, C. Cavazzoni, D. Ceresoli, G. L. Chiarotti, M. Cococcioni, I. Dabo, A. Dal Corso, S. de Gironcoli, S. Fabris, G. Fratesi, R. Gebauer, U. Gerstmann, C. Gougoussis, A. Kokalj, M. Lazzeri, L. Martin-Samos, N. Marzari, F. Mauri, R. Mazzarello, S. Paolini, A. Pasquarello, L. Paulatto, C. Sbraccia, S. Scandolo, G. Sclauzero, A. P. Seitsonen, A. Smogunov, P. Umari and R. M. Wentzcovitch, *J. Phys.: Condens. Matter*, 2009, **21**, 395502.
42 J. Barrio and M. Shalom, *ChemCatChem*, 2018, **10**, 5573–5586.
43 J. Zhuang, W. Dai, Q. Tian, Z. Li, L. Xie, J. Wang, P. Liu, X. Shi and D. Wang, *Langmuir*, 2010, **26**, 9686–9694.
44 U. I. Gaya and A. H. Abdullah, *J. Photochem. Photobiol., C*, 2008, **9**, 1–12.
45 Y. Shiraishi and T. Hirai, *J. Photochem. Photobiol., C*, 2008, **9**, 157–170.
46 L. Li, M. Shalom, Y. Zhao, J. Barrio and M. Antonietti, *J. Mater. Chem. A*, 2017, **5**, 18502–18508.
47 J. Barrio, N. Karjule, J. Qin and M. Shalom, *ChemCatChem*, 2019, **11**, 6295–6300.